Astronomy & Astrophysics manuscript no. ferrigno˙4U0115
February 25, 2009

Study of the accreting pulsar 4U 0115+63 with a bulk and thermal Comptonization model

Carlo Ferrigno[1,2], Peter A. Becker[3], Alberto Segreto[4], Teresa Mineo[4], and Andrea Santangelo[2]

[1] ISDC chemin d'Écogia, 16 1290 Versoix Switzerland
e-mail: Carlo.Ferrigno@unige.ch
[2] IAAT, Abt. Astronomie, Universität Tübingen, Sand 1, 72076 Tübingen, Germany
[3] Department of Computational and Data Sciences
George Mason University
4400 University Drive, MS 6A3 Fairfax, VA 22030
[4] IASF-INAF, via Ugo la Malfa 153, 90146 Palermo Italy

Received —; accepted —

Abstract

Context. Highly magnetized pulsars accreting matter in a binary system are bright sources in the X-ray band (0.1–100 keV). Despite the early comprehension of the basic emission mechanism, their spectral energy distribution is generally described by phenomenological or simplified models.
Aims. We propose a study of the spectral emission from the high mass X–ray binary pulsar 4U 0115+63 by means of thermal and bulk Comptonization models based on the physical properties of such objects.
Methods. For this purpose, we analyze the *BeppoSAX* data in the energy range 0.7–100 keV of the 1999 giant outburst, 12 days after the maximum. We focus first on the phase averaged emission, and then on the phase resolved spectra, by modeling the system using a two-component continuum.
Results. At higher energy, above ~ 7 keV, the emission is due to thermal and bulk Comptonization of the seed photons produced by cyclotron cooling of the accretion column, and at lower energy, the emission is due to thermal Comptonization of a blackbody source in a diffuse halo close to the stellar surface. Phase resolved analysis establishes that most of the emission in the main peak comes from the column, while the low energy component gives a nearly constant contribution throughout the phase.
Conclusions. From the best fit parameters, we argue that the cyclotron emission is produced ~ 1.7 km above the stellar surface, and escapes from the column near its base, where the absorption features are generated by the interaction with the magnetic field in the halo. We find that in 4U 0115+63, the observed spectrum is dominated by reprocessed cyclotron radiation, whereas in other bright sources with stronger magnetic fields such as Her X-1, the spectrum is dominated by reprocessed bremsstrahlung.

Key words. X-rays: binaries, pulsars: individual: 4U 0115+63

1. Introduction

X–ray binary pulsars (XRBPs) were discovered more than 35 years ago with the pioneering observations of the bright sources Her X-1 (Giacconi et al. 1971) and Cen X-3 (Tananbaum et al. 1972). The basic mechanisms of the pulsed emission were understood quickly: radiation originates from the accretion of ionized gas onto a rotating neutron star (NS) from a nearby companion, an O or B star ($M \geq 5M_{\odot}$) in high mass X-ray binaries (HMXBs), a later than type A star ($M \leq M_{\odot}$) in low mass X-ray binaries. For strong magnetic fields ($B \sim 10^{11-12}$ G) of the compact object, the plasma is threaded at several hundred stellar radii and then funneled along the magnetic field lines onto the magnetic poles, forming one or two accretion columns (Pringle & Rees 1972; Davidson & Ostriker 1973). The system is powered by the conversion of gravitational potential energy into kinetic energy, which is eventually emitted in the form of X-rays as the plasma decelerates, possibly through a radiative shock, and settles onto the stellar surface. Pulsation is generated because of the nonalignment between the magnetic and rotational axes.

The spectral emission from XRBPs still presents many puzzling aspects. Recently, Becker & Wolff (2007) made a major step forward by proposing a model (from here on the BW model) which represents a complete calculation of the X-ray spectrum associated with the physical accretion scenario first suggested by Davidson & Ostriker (1973). A summary of the model properties will be given in Sect. 2

A unique spectral characteristic of many HMXBs is the presence of cyclotron resonant scattering features (CRSFs), which provide a tool for direct measurement of the magnetic-field strengths of accreting pulsars, a key ingredient of the model. The fundamental line appears at $E_{\rm cyc} = 11.6\, B_{12} \times (1+z)^{-1}$ keV, where B_{12} is the magnetic field strength in units of 10^{12} G and z is the gravitational redshift in the line-forming region (Wasserman & Shapiro 1983). However, the determination of the centroid energy of the fundamental line might be hampered by its complex shape, due to photon spawning (see e.g. Kreykenbohm et al. 2005). The second harmonic is deeper and can be described by a simple analytical function such as a Gaussian curve, since it is due to pure absorption (Nishimura 2003). Phase resolved spectral analysis is essential for this kind of study because the spectral characteristics of the lines depend heavily on the angle between the observation direction and

Send offprint requests to: C. Ferrigno

the magnetic field orientation (see e.g. Araya & Harding 1999; Araya-Góchez & Harding 2000; Schönherr et al. 2007).

In this paper we use the BW model to study an observation of the bright HMXB 4U 0115+634. Hard X-ray radiation from this source was discovered in 1969 (Whitlock et al. 1989), during one of its giant type II outbursts (16 have been observed up to now), when the X-ray luminosity rises to a few 10^{37} erg/s, two orders of magnitude above its quiescent level. X-ray pulsations ($P_S = 3.6$ s) were soon discovered (Cominsky et al. 1978), and the determination of the orbital parameter ($P_{\rm orb} = 24.3$ d, $e = 0.34$, $a_X \sin i = 140.1$ lt − s) was made possible for the first time using the *SAS* data (Rappaport et al. 1978). The high energy ($\gtrsim 10$ keV) continuum of 4U 0115+63 has previously been modeled with the standard power-law modified by an exponential cut-off (e.g. Coburn et al. 2002). The source has also been widely studied in the optical and IR bands, allowing the identification of its optical counterpart, V 635 Cas (Johns et al. 1978), and also the determination of its distance 7–8 kpc (Negueruela & Okazaki 2001).

In the spectrum of 4U 0115+63, cyclotron harmonics have been observed up the fifth order (Wheaton et al. 1979; White et al. 1983; Heindl et al. 1999; Santangelo et al. 1999), while in the other known XRBPs, only the second harmonic, and in one case the third (Tsygankov et al. 2006), is sometimes detected (Coburn et al. 2002; Orlandini 2004; Caballero et al. 2007). The luminosity of 4U 0115+63 during outburst is comparable to that of the bright sources Her X-1 and Cen X-3 studied by BW, but the magnetic field strength, $\sim 10^{12}$ G, implied by the cyclotron absorption features in the spectrum of 4U 0115+63 is considerably lower than the field strength in the other two sources. As a result of the analysis presented here, we find that the decrease in the field strength causes a fundamental shift in the character of the emitted X-ray spectrum, from Comptonized bremsstrahlung in Her X-1 and Cen X-3 to Comptonized cyclotron in 4U 0115+63.

The relation between the optical properties of the system and the X-ray type II outbursts have been studied by Whitlock et al. (1989), who suggested a 3-year quasi-periodicity of the outbursts. Later, Negueruela & Okazaki (2001) and Negueruela et al. (2001) were able to characterize the outburst mechanism as a result of a disc instability due to radiative warping.

The *GINGA* observations evidenced how both the continuum and the line energies are phase-dependent (Mihara et al. 2004). A remarkable result, obtained analyzing the *RXTE* data, is the luminosity dependence of the cyclotron features (Nakajima et al. 2006). This is interpreted as reflecting the passage from a radiation-dominated flow with a shock above the stellar surface at high luminosity, to a matter-dominated flow at low luminosity, in which the accreting material is brought to rest at the stellar surface by the pressure of the gas. Additional constraints on the height of the line forming region in 4U 0115+63 have been developed by Tsygankov et al. (2007), who also concluded that the height of the hard-photon emission region in the column decreases with decreasing luminosity.

After providing a brief summary of the Becker & Wolff (2007) column emission model, in Sect. 3 we describe the observations and the analysis methods. In Sect. 4 we report our results, which are discussed in detail in Sect. 5. Finally, in Sect. 6, we draw our conclusions.

2. Summary of the column emission model

Becker & Wolff (2007) proposed a model for the production of the accretion column emission spectrum based on the bulk and thermal Comptonization of seed photons emitted via bremsstrahlung, cyclotron, and blackbody processes occurring in the accreting plasma. The partial differential equation governing the Green's function yields an analytical solution that can be convolved with the seed photon distribution to produce an emergent spectrum displaying a power-law continuum with an exponential cutoff at high energies. They assume a cylindrical geometry for the column, along with a constant electron temperature and a constant magnetic field. The constant properties of the column are a reasonable approximation, since most of the relevant interactions are thought to take place in a relatively thin layer close to its base. The density and velocity profiles of the infalling matter are analytical approximations of numerically computed functions, and the angle-dependent cross section is approximated using two terms to represent the mode-averaged electron scattering cross sections for photons propagating either parallel or perpendicular to the magnetic field direction, denoted by ($\sigma_\parallel$) and ($\sigma_\perp$), respectively.

The cyclotron and bremsstrahlung source distributions each vary as the square of the plasma density, but their energy dependences are quite different: the cyclotron emission is due to the collisional excitation and radiative decay of the first Landau level, and it therefore displays a monoenergetic energy dependence; the bremsstrahlung emission is due to the braking of electrons interacting with protons, and it therefore possesses a continuous energy dependence. The combination of these terms provides a good approximation of the free-free process in very strong magnetic fields (Riffert et al. 1999). It should be emphasized that when the cyclotron energy is comparable to the plasma temperature, the cyclotron emission becomes the preferred cooling channel (Arons et al. 1987). Finally, blackbody emission is localized at the base of the column due to the presence of the thermal mound; it is the only term for which an integral must be numerically computed to derive the emergent spectrum.

For given values of the stellar mass M_* and the stellar radius R_*, the BW model has six fundamental free parameters, namely the accretion rate $\dot{M}$, the column radius r_0, the electron temperature T_e, the magnetic field strength B, the photon diffusion parameter ξ, and the Comptonization parameter δ, with the final two parameters are defined by

$$\xi = \frac{\pi r_0 m_p c}{\dot{M}\left(\sigma_\parallel \sigma_\perp\right)^{1/2}} , \quad \frac{\delta}{4} = \frac{y_{\rm bulk}}{y_{\rm thermal}} , \tag{1}$$

where m_p denotes the proton mass, c is the speed of light, and $y_{\rm bulk}$ and $y_{\rm thermal}$ represent the y-parameters[1] for the bulk and thermal Comptonization processes.

The accretion rate is constrained by the observed luminosity, under the assumption of isotropic accretion and unitary efficiency, which might allow us to remove this parameter from the set. A unique solution for the remaining free parameters can be found by comparing the model spectrum with the observations for a particular source. The analytical nature of the model makes it amenable to incorporation into standard analysis packages such as `Xspec`, as we did, which facilitates observational testing.

[1] The y-parameters describes the average fractional energy change experienced by a photon before it escapes through the column walls.

3. Observations and data analysis.

This work is based on the observations performed by *BeppoSAX* (see Boella et al. 1997a, for a description of the mission) on 1999 March, 26 at 17:31:32.5 (OP6714) and ended on 1999 March, 27 at 17:34:05.5, during the decay of a giant outburst, more precisely 12 days after the peak, when the flux in the 2–10 keV energy range was a factor of two lower than the maximum value (see Fig. 1 of Heindl et al. 1999). Among the many publicly available observations of 4U 0115+63 during its X-ray outbursts, our choice is driven by the wide energy band, good spectral resolution, and reliable calibration of the *BeppoSAX* instruments, and also by the relatively long exposure of this dataset. Another observation of the same outburst, made seven days earlier, is reported in Santangelo et al. (1999).

We analyze the data obtained by the high energy narrow field instruments *LECS* (0.7–4.0 keV, Parmar et al. 1997), *MECS* (1.5–10.5 keV, Boella et al. 1997b), *HPGSPC* (7–44 keV, Manzo et al. 1997) and *PDS* (15–100 keV, Frontera et al. 1997) after the processing through the standard pipeline (`saxdas` v.2.1). Background subtraction is performed using the Earth occultation for *HPGSPC*, the off-source pointing for *PDS*, and the standard calibration files for *MECS* and *LECS*. The *LECS* and *MECS* source extraction radii are set to 8′ for an optimal signal to noise ratio. The instrument exposure times are 5043 s (*LECS*), 53 660.4 s (*MECS*), 42 495.3 s (*HPGSPC*), and 48 328.9 s (*PDS*), with the differences due to the variations in the operating procedures.

3.1. Spectral analysis

The spectral analysis is performed with the `Xspec` package version 12.3.1 (Arnaud 1996), using our implementation of the analytical model for the vertically-integrated accretion column emission spectrum developed by Becker & Wolff (2007). The fundamental and harmonic cyclotron resonant absorption features are modeled using multiplicative Gaussian functions:

$$G(E) = \left(1 - \frac{N_n}{\sigma_n \sqrt{2\pi}} e^{-\frac{1}{2}\left(\frac{E-E_{cn}}{\sigma_n}\right)^2}\right), \qquad (2)$$

where N_n, E_{cn}, and σ_n denote the strength, energy, and standard deviation of the absorption function for the nth harmonic. The line width is fixed whenever it cannot be determined by the fit; this is always the case for the fourth and fifth harmonics, set to the convenient value of 4 keV.

The phase averaged spectrum is studied at first, then we divide the pulse period into 15 bins of equal width and analyze each spectrum separately to obtain the dependency of the parameters on the phase. Due to the short exposure, we use the *LECS* data only in the phase averaged spectrum. All of the errors are reported at 90% confidence level (c.l.), i.e. $\Delta\chi^2_{\rm min} = 2.7$ for one parameter of interest, unless stated differently.

3.2. Timing analysis

We transform the photon arrival times into the Solar system barycenter reference frame using the standard tool for *BeppoSAX* (`baryconv`), then to the binary system reference frame using the ephemeris (Rappaport et al. 1978; Tamura et al. 1992). Using the *HPGSPC* data, we find the pulse period $P = 3.614246 \pm 0.000002$ s on 1999-03-26 at 17:28:45.643 UT (MJD 51263.72830605) adopting the phase shift method described by Ferrigno et al. (2007). I.e. we divide the observation into 174 equally spaced time bins; in each bin, we determine the phase of the pulse maximum with a typical uncertainty of 5% and then linearly fit these values as functions of time by adapting iteratively the initial guess on the period. The quoted uncertainty is purely statistical. If no orbital correction is applied, we find a significant variation of the pulse period within the observation: $\dot{P} = (2.6904 \pm 0.0005) \times 10^{-9}$ s/s.

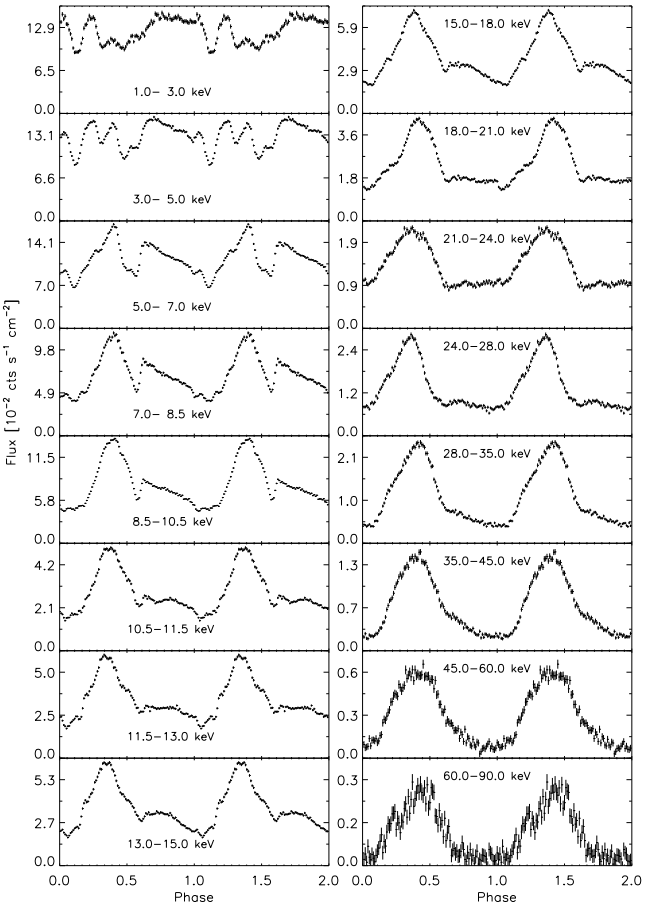

Figure 1. Pulse profiles of 4U 0115+63 in different energy ranges. The data are from the *MECS* (1.0–8.5 keV), *HPGSPC* (8.5–28 keV) and *PDS* (28–95 keV) instruments on board of *BeppoSAX*.

We fold the light curves in different energy ranges with 100 phase bins (Fig. 1). To account for the timing systematics of the three instruments the pulse profiles are arbitrarily shifted to obtain an optimal alignment in the common energy ranges (8–11 keV for *MECS* and *HPGSPC*, 20–25 keV for *HPGSPC* and *PDS*): we apply a forward phase shift of 4 bins (∼0.14 s) to the *MECS* profiles and of 5 bins (∼0.18 s) to the *PDS* ones keeping the *HPGSPC* profiles as reference. The reason for this instrumental timing problem is currently unknown.

4. Results

4.1. Pulse profiles

The shape of the pulse profiles, shown in Fig. 1, is highly variable with energy: above ∼ 10 keV we can clearly distinguish a main peak at pulse phase ∼ 0.4, and, with more attention, a sec-

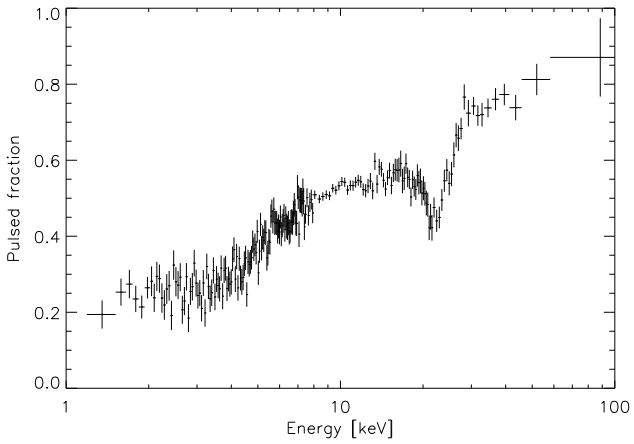

Figure 2. Pulsed fraction as function of energy, from 1.2 to 8 keV the data are from MECS, from 8 to 30 keV from *HPGSPC*, and from 30 to 120 keV from *PDS*.

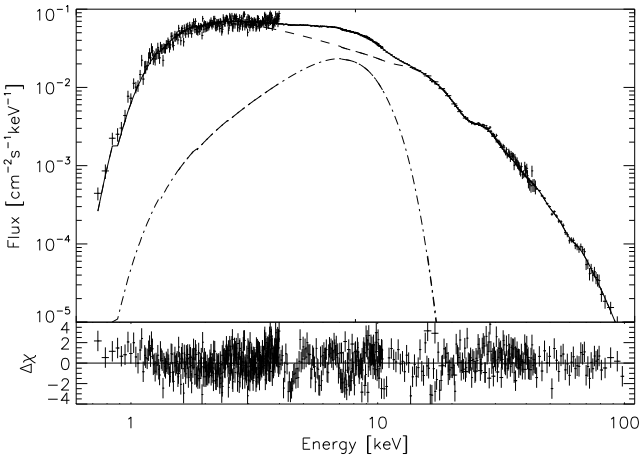

Figure 3. Upper panel: the unfolded spectrum of 4U 0115+63 described by the phenomenological model: the dashed line is the high-energy cut-off power law, the dot-dashed line the broad Gaussian, and the solid line the sum. The spectra of the four instruments have been scaled according to the inter-calibration constants of Table 1. Lower panel: residuals from the best fit model.

Table 1. Instrument inter-calibration constants using the *HPGSPC* as reference.

Instrument	Constant
LECS	0.814± 0.008
MECS	0.970± 0.003
PDS	0.857± 0.004

ondary shallower one at pulse phase ~ 0.7 interpreted by some authors as the partially obscured emission of the column of the opposite polar cap (Tsygankov et al. 2007). Below this energy, the pulse shape is more complex, suggesting that the lower energy emission is generated by a different mechanism.

We compute the pulsed fraction, i.e. the ratio $\frac{F_{\max}-F_{\min}}{F_{\max}+F_{\min}}$, as a function of energy, where the count rates at the maximum ($F_{\max}$) and minimum ($F_{\min}$) of the pulses are the weighted average of three neighboring phase bins. We perform an energy binning, which ensures that the signal is at least 140 times larger than the noise for each pulse profile.

As shown in Fig. 2, the pulsed fraction below 5 keV remains always between 20% and 30%, then it begins to raise, showing at ~ 22 keV a sharp localized decrease due to the resonant scattering at the second Landau level. The low S/N at high energy prevents the detection of the higher harmonics, and even the fundamental cannot be clearly identified despite the high count level. This may be due to competing effects such as photon spawning and cyclotron emission. We verified that in the overlapping energy ranges, the data of the three instruments are consistent with each other.

4.2. Phase averaged spectrum

Due to the well-known problems in the absolute calibration, we used inter-calibration constants between the different instruments: they are obtained from a best fit procedure setting the *HPGSPC* as reference. We verified that the results reported in Table 1 are model independent (within the quoted errors) and consistent with the instrument team recommendations.[2]

[2] http://heasarc.gsfc.nasa.gov/docs/sax/abc/saxabc/saxabc.html

4.2.1. Phenomenological model

The aim of this work is the introduction of a physical model to describe the spectrum. However, we study the traditional phenomenological models for comparison with the results present in the literature. The fit with a simple high-energy cut-off power law plus absorption features is unsatisfactory ($\chi^2_{\rm red} = 2.4$); we then adopt the model that Klochkov et al. (2008) applied to the high mass X-ray binary EXO 2030+375: a broad Gaussian emission line plus a high-energy cut-off power-law. The absorption lines are described by eq. (2), photoelectric absorption by the model `phabs` in `Xspec`.

The unfolded spectrum is reported in Fig. 3 and the best fit parameters in Table 2: the continuum is altered only locally by cyclotron resonances, the fundamental line is shallower than the second harmonic as expected from the pulsed fraction of Fig. 2, and the photon index is almost equal to one, as typical for saturated Comptonization (Coburn et al. 2002). The photoelectric absorption is parametrized by $N_{\rm H} = (1.38 \pm 0.03) \times 10^{22}\,{\rm cm}^{-2}$, which is higher than the value for Galactic absorption in the source direction, $N_{\rm H,Gal} = 0.9 \times 10^{22}\,{\rm cm}^{-2}$, (average of the values of Dickey & Lockman 1990; Kalberla et al. 2005), thus the X-ray emission seems to be attenuated also locally around the source.

We derive a flux in the 1-100 keV band of $(1.69 \pm 0.02)\,{\rm erg\,s^{-1}\,cm^{-2}}$ corresponding to a luminosity $L_X = 6.3 \times 10^{37}\,{\rm erg\,s^{-1}}$ assuming a distance of 7 kpc. In this model, the power-law component is responsible for the high- and low-energy portions of the spectrum, which are characterized by completely different pulse profiles. The "bump" below the cyclotron energy is described by the broad Gaussian line, which does not correspond clearly to any physical process.

4.2.2. Comptonization model

If we apply the model proposed by Becker & Wolff (2007), using as an input parameter the magnetic field derived using the

cyclotron absorption features, then the Comptonized cyclotron emission has a flux about two orders of magnitude larger than the bremsstrahlung and blackbody components, and the resulting spectrum does not reproduce the lower energy portion of the 4U 0115+63 spectrum. Driven by the observation that the pulse profiles below $\sim$ 5 keV are very different from the others, we therefore try to fit the spectrum below this energy with another component. The attempts to use a blackbody, a cut-off power law, or a simple power-law, all attenuated by photo-electric absorption, are unsuccessful, giving $\chi_{\rm red} \gtrsim 2.5$. Among the reasonably simple models, only the thermal Comptonization of low energy (0.1–0.5 keV) blackbody emission, located in the center of a spherical cloud of hot electrons, gives a satisfactory fit to the data, as verified by the application of the `compST` (Sunyaev & Titarchuk 1980) and `compTT` (Titarchuk 1994) models in `Xspec`. We will therefore attempt to fit the broad band spectrum of 4U 0115+63 using a combination of the BW bulk+thermal Comptonization model, which gives good agreement at high energies, and a thermal Comptonization component at lower energy. As discussed below, we interpret the low energy component as emission arising in a halo of gas surrounding the base of the accretion column.

From the statistical point of view, it is not possible to discriminate between the thermal Comptonization models for the low energy component. We then compute the effective radius of the blackbody which produces the seed photons following the method of in 't Zand et al. (1999). In the `compST` model, the temperature of the seed photons is fixed to 0.1 keV: for best fit parameters of the hot electron temperature T_e = (2.91 ± 0.04) keV, the optical depth of the spherical cloud τ = 22.2 ± 0.4, and the 2-100 keV flux for this spectral component of 5.13×10^{-9} erg cm^{-2}s^{-1}, the blackbody radius is 550 km, which is clearly too high for such a system. We therefore utilize the `compTT` model rather than the `compST` model to analyze the low-energy component.

Using the `compTT` model, it is possible to determine the seed photon temperature, T_0 = (0.51 ± 0.01) keV, if we fix the absorption column to the Galactic value. In this scenario, the low energy emission is produced by an optically thick plasma halo (τ = 24.4 ± 0.4) at temperature T_C = (2.90 ± 0.04) keV, while for comparison the BW electron temperature in the column is T_e = (7.94 ± 0.11) keV. With these parameters (reported in Table 2), corresponding to a flux in the 0.5–100 keV band of 5.19×10^{-9} erg cm^{-2}s^{-1}, we obtain a blackbody effective radius of ∼16 km, which is of the right order of magnitude. Assuming a standard NS, the gravitational redshift at the surface is 0.3. Correcting for this effect, we find best-fit parameters corresponding to a blackbody with ∼9 km radius. However, in the rest of the paper we will neglect the relativistic effects for consistency with the BW model.

If we fix the magnetic field strength of the BW component using the value derived from the absorption lines, then we find there is no combination of the other parameters which can account for the emission between $\sim$ 7 and $\sim$ 10 keV. We therefore leave the magnetic field in the BW component as a free parameter, which effectively separates the spatial region where the high-energy BW component is produced from the region where the cyclotron absorption features are imprinted on the emergent spectrum. The implications of this physical picture are further discussed below. The mass accretion $\dot{M}$ is also determined through the spectral fit. Since there is a very strong correlation between the column radius r_0 and $\dot{M}$, we study the contour plot of r_0 and $\dot{M}$ and find that a good fit is obtained for $r_0 \simeq 600$ m and $\dot{M} \simeq 0.6 \times 10^{17}$ g/s. The value obtained for the accretion rate

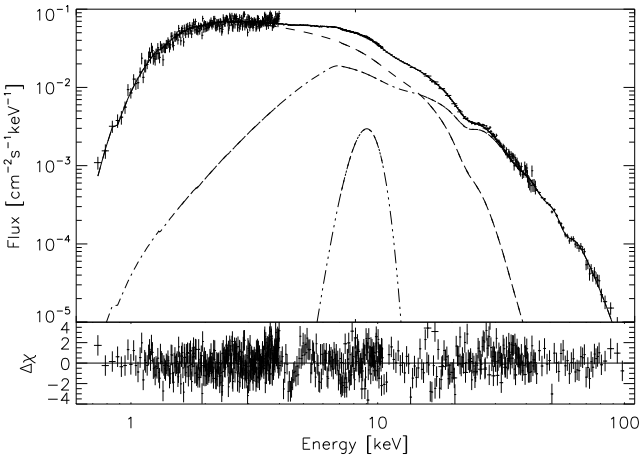

Figure 4. Upper panel: the unfolded spectrum of 4U 0115+63 described by the Comptonization model: the dashed line is the thermal Comptonization, the dot-dashed line the column emission computed using the BW model, the dot-dot-dashed line a narrow Gaussian line, and the solid line the sum. The spectra of the four instruments have been scaled according to the inter-calibration constants of Table 1. Lower panel: residuals from the best fit model.

using the fit is somewhat lower than that expected if the emission were isotropic, in which case the X-ray luminosity would imply $\dot{M} = 3.3 \times 10^{17}$ g/s. Our result for $\dot{M}$ therefore suggests that the emission from the column is anisotropic, as expected for a fan beam. This point is further discussed in Sect. 5.

We then freeze r_0 and $\dot{M}$ to obtain a stable fit for the other model parameters, and the neutron star mass and radius are fixed at the standard values of 1.4 $M_\odot$ and 10 km, which cannot be constrained by the comparison to the data. Among the results reported in Table 2, we note that the magnetic field which produces the cyclotron emission in the BW model has a strength $B = (5.91 \pm 0.02) \times 10^{11}$ G while the line centroid energy implies that the magnetic field in the line forming region is $\sim 10^{12}$ G. These results clearly suggest the existence of a spatial offset between the BW emission region and the cyclotron absorption region, as further explored in Sect. 5.

Due to some residuals in the transition region between the low energy thermal Comptonization component and the BW column emission, we introduce a third emission component in the form of a Gaussian line with energy $\sim$ 9 keV and standard deviation σ = 1 keV. From Fig. 4 it is clear that this component gives a negligible contribution to the flux, unlike in the phenomenological model, and its necessity here probably stems from our rough description of the cyclotron scattering in strong magnetic fields.

4.3. Phase resolved spectroscopy

The vertically-integrated accretion column emission spectrum computed using the BW model is independent of the observation angle of the observer, who is assumed to be at rest in the frame of the neutron star. The angle independence stems from the fact that the model does not incorporate the full angle and energy dependence of the cyclotron scattering cross section, but instead uses a two-component formalism based on the cross sections ($\sigma_\parallel$) and ($\sigma_\perp$) for photons propagating either parallel or

Table 2. Best fit parameters of the phase averaged spectral model, if uncertainties are omitted, the parameter is frozen.

Phenomenological		Physical	
$N_{\rm H}$ [cm^{-2}]	1.38±0.03	$N_{\rm H}$ [cm^{-2}]	0.9
		T_0 [keV]	0.51±0.01
		T_C [keV]	$2.90^{+0.03}_{-0.05}$
		τ	24.4±0.4
		norm*	0.257±0.003
E_c [keV]	14.5±0.3	ξ	$4.0^{+0.2}_{-0.4}$
E_f [keV]	13.5±0.2	δ	0.59±0.02
Γ	0.998±0.007	B[10^{12}G]	0.591±0.002
K	0.247±0.003	T_e [keV]	7.94±0.11
		r_0 [m]	600
		$\dot{M}$ [10^{17}g s^{-1}]	0.6
E_G [keV]	$7.056^{0.014}_{-0.029}$	E_G [keV]	9.07±0.12
σ_G [keV]	$2.51^{+0.08}_{-0.03}$	σ_G [keV]	1
N_G [cts cm^{-2} s^{-1}]	0.144±0.003	N_G [cts cm^{-2} s^{-1}]	0.0080±0.0009
E_1 [keV]	11.16±0.15	E_1 [keV]	11.58±0.13
σ_1 [keV]	1	σ_1 [keV]	2
N_1 [cts keV]	0.09±0.02	N_1 [cts keV]	0.70±0.04
E_2 [keV]	22.99±0.05	E_2 [keV]	22.76±0.09
σ_2 [keV]	2.8±0.1	σ_2 [keV]	2
N_2 [cts keV]	2.3±0.1	N_2 [cts keV]	1.22±0.05
E_3 [keV]	32.6±0.4	E_3 [keV]	36.3±0.6
σ_3 [keV]	3	σ_3 [keV]	3
N_3 [cts keV]	1.6±0.2	N_3 [cts keV]	2.4±0.2
E_4 [keV]	40.8±0.7	E_4 [keV]	46.5±1.1
σ_4 [keV]	4	σ_3 [keV]	4
N_4 [cts keV]	2.5±0.2	N_4 [cts keV]	2.9±0.4
E_5 [keV]	53±1	E_5 [keV]	57±2
σ_5 [keV]	4	σ_3 [keV]	4
N_5 [cts keV]	2.6±0.4	N_5 [cts keV]	3.6±0.7
χ^2 (d.o.f.)	1.48(705)	χ^2 (d.o.f.)	1.49(703)
flux**	$(1.070\pm0.002)\times10^{-8}$	flux**	$(1.070\pm0.003)\times10^{-8}$

* the definition of the model normalization is reported in `Xspec` documentation.
** the flux in the 1-100 keV energy band is expressed in units of erg cm^{-2} s^{-1}.

perpendicular to the field. Despite the simplified treatment of the scattering cross section, it is interesting to see what insight can be gained by fitting the BW model to the phase-resolved spectral data. Physically, variations in the phase-resolved spectrum arise due to the partial occultation of the base of the accretion column, in combination with the angle dependence of the cyclotron cross section. These physical effects can be studied in an approximate manner by allowing the parameters in the BW model to vary as functions of the pulse phase. For example, the effect of the changing angle of observation due to the pulsar spin can be modeled by allowing the cross sections ($\sigma_\parallel$) and ($\sigma_\perp$) to vary, resulting in variation of the parameter ξ as a function of the pulse phase (see eq. [1]). Conversely, the effect of the partial occultation of the base of the column can be modeled by allowing for a phase dependency in the parameters B, T_e, and δ. Moreover, in each phase bin we note that light bending (see e.g. Kraus et al. 2003) might cause the mixing of emission arriving from different angles. Based on these observations, we extract phase-dependent parameters by applying the BW model to the spectra in 15 equally spaced phase bins.

For the BW component, we adopt the values of $\dot{M}$ and r_0 derived for the phase averaged spectrum. For the lower energy `compTT` component, since we do not use the *LECS* data, the temperature of the seed photons cannot be constrained; we therefore freeze it to the value 0.51 keV found in the phase averaged spectrum. Depending on the particular characteristics of each single spectrum, some parameters cannot be constrained and thus are frozen at a suitable value consistent with the neighboring bins or the phase averaged spectrum. In particular, we put great care in limiting the line width by freezing the σ parameter in the fitting process whenever its unconstrained value would give a major contribution to the continuum model.

We also allow a fine tuning of the relative normalization between the different instruments due to the uncertainty in the absolute timing for *BeppoSAX* (see Sect. 3). However, we verified that the scatter is within 8% (*PDS*) and 3% (*MECS*) from the values computed for the phase averaged spectrum and reported in Table 1. Eventually, we obtained for the fits reduced χ^2 between 0.94 and 1.2 for 346–352 degrees of freedom corresponding to a null hypothesis probability always lower than 0.5%. Given the model uncertainties, we consider this an acceptable result. The unfolded spectra are reported in Fig. 5.

The phase dependency of the best fit parameters in the BW component is shown in Fig. 6: the magnetic field B is higher at the edges of the main peak (phase 0.13–0.66), as is the contribution of bulk with respect to thermal Comptonization described by the parameter δ. The parameter ξ follows roughly the luminosity phase dependency, whilst the temperature of the electrons T_e displays a single peak at phase ~ 0.5. The pattern is less clear outside the main peak and will not be discussed further.

The phase dependency of the optical depth τ and electron temperature T_C in the lower energy `compTT` component is shown in Fig. 7: the former is always very high, between 20 and 35, and the latter varies almost by a factor of three. Even though the

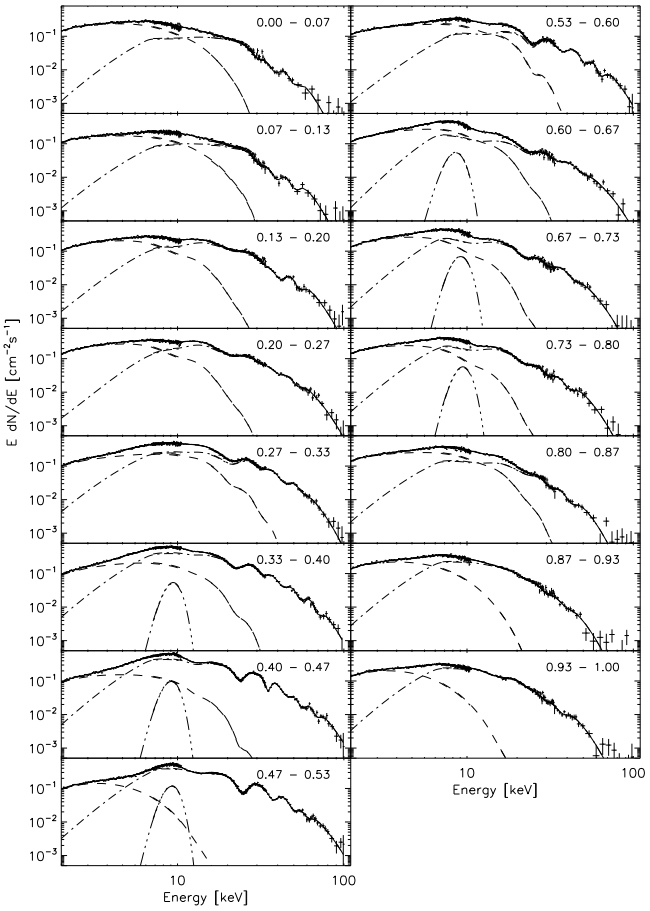

Figure 5. Unfolded phase resolved spectra. The phase range is indicated in each plot. The dashed line is the thermal Comptonization, the dot-dashed line the column emission computed using the BW model, the dot-dot-dashed line a narrow Gaussian line, and the solid line the sum.

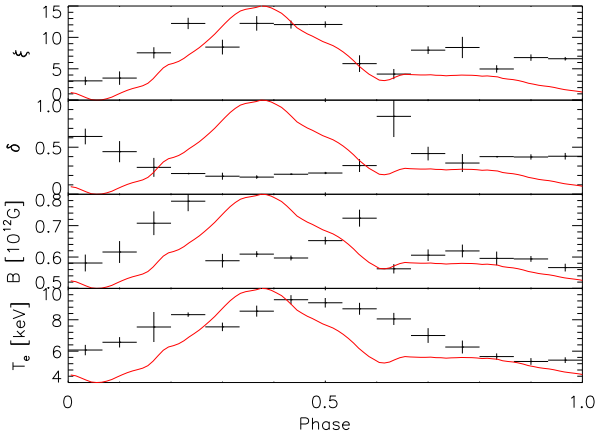

Figure 6. Best fit parameters for the Becker and Wolff spectral component as function of the phase. The accretion column radius is fixed at 600 m and the mass accretion rate at 6×10^{16} g s^{-1}. The solid line is the smoothed pulse profile in the 10–20 keV energy band with arbitrary normalization.

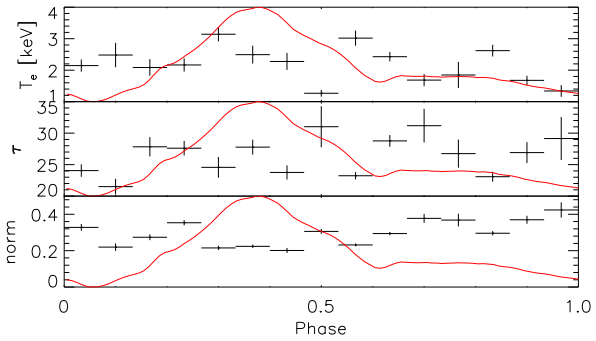

Figure 7. Best fit parameters for the soft Comptonization spectral component (compTT) as function of the phase. The temperature of the seed photons is fixed to 0.51 keV. The solid line is the smoothed pulse profile in the 10–20 keV energy band with arbitrary normalization.

deviation from a constant value is highly significant for both parameters, there are no clear correlations with the pulse structure. The additive Gaussian line has always a centroid energy around 9 keV with no obvious correlation to the magnetic field intensity (Fig. 8), however its minimal presence is required to obtain an acceptable χ^2 in six phase bins.

We show in Fig. 9 the centroid energies, the width of the first three harmonics, the line normalization, and the ratio between the centroid energies and half the centroid energy of the second harmonic. This final parameter can be considered the best indicator of the magnetic field intensity in the line forming region, since the second harmonic is purely due to scattering and, incidentally, it is covered with high S/N by two instruments in this observation. We note that along the main peak (phase 0.12–0.66), the higher harmonics are almost equally spaced: the deviations are at most of 4% with less than 3σ significance. Note that for the same phase range, the fundamental is systematically higher, and from phase 0.66 to 1.12, the lines do not present a regular spacing.

4.4. Search for higher harmonics

At phase 0.33–0.46 (the peak), we introduce a previously undetected *sixth harmonic* to model some residuals in the high-energy tail of the spectrum. To have a better grasp on the line significance and verify it is not due to an inappropriate modeling of the continuum, we test its presence using a cut-off power model for the energy range above 13 keV. This model was used for previous analyses (see e.g. Santangelo et al. 1999). The results are reported in Table 3: the probability that the feature is only a statistical fluctuation is not negligible, therefore we cannot claim a firm detection of the sixth harmonic, just a strong suggestion of its presence since the centroid energy is compatible with the value of the second harmonic, the line normalization is greater than zero at 90% c.l., and it is present in two distinct phase bins at the pulse maximum.

Table 3. Fit results in the search for the 6th harmonic using the cut-off power law model for the continuum above 13 keV. $\Delta\chi^2$ is referred to the introduction of the further Gaussian absorption line. $E_{\rm abs}$ is the centroid value, E_B is the value corresponding to three times the centroid energy of the second harmonic, and Nabs is the line normalization. The null hypothesis probability is obtained using the F-test.

phase	0.33–0.40	0.40–0.46
$E_{\rm abs}$ [keV]	71 ± 3	68.6 ± 2.6
E_B [keV]	66.9 ± 0.3	70.74 ± 0.15
$N_{\rm abs}$ [keV]	4.5 ± 2.5	$3.1^{+1.3}_{-0.6}$
$\Delta\chi^2$(d.o.f.)	221(168) → 215(166)	158(142) → 152(140)
Null hypothesis probability	10%	5%

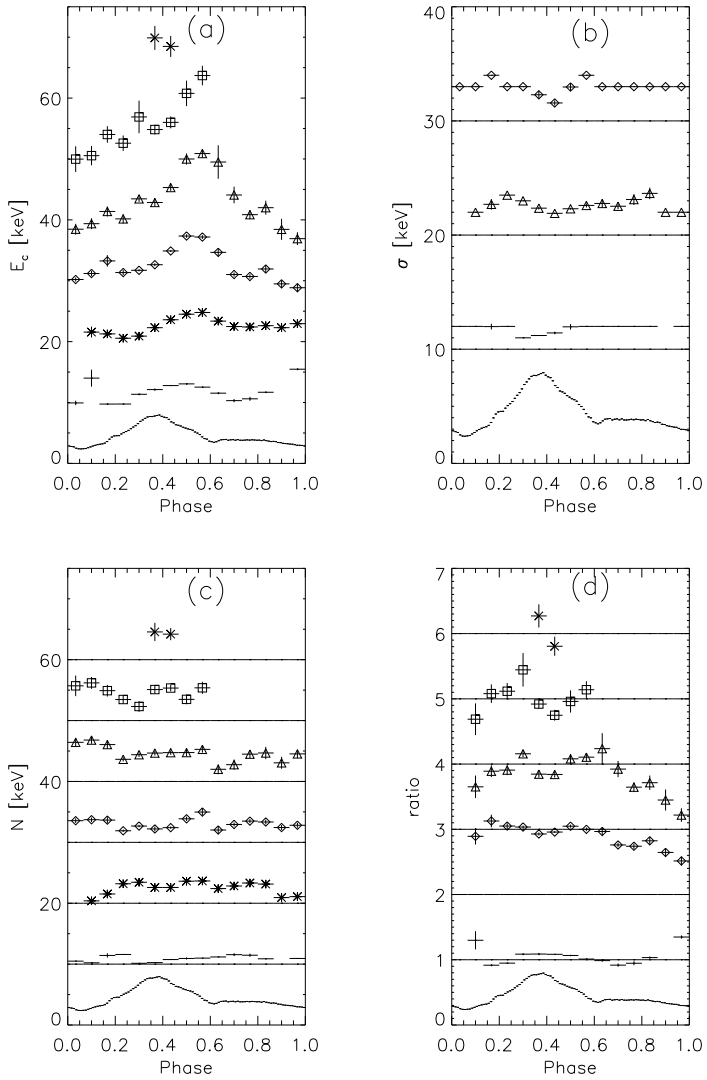

Figure 9. Absorption line parameters. (a) The centroid energy. (b) The width. (c) The normalization. (d) The ratio between the centroid energy and half the centroid energy of the second harmonic. In each plot the 10-20 keV pulse profile is sketched with arbitrary normalization for illustrative purpose. Line width and normalization are vertically displaced of 10n keV, where n is the harmonic order. Uncertainties are reported at 1σ c.l. assuming a Gaussian symmetric distribution.

5. Discussion

We have applied the self-consistent bulk+thermal Comptonization model developed by Becker & Wolff (2007) to study the bright transient source 4U 0115+63. In order to treat this source, we find that the BW model needs some adjustments with respect to the prescriptions in the original paper. The first issue is the relatively low accretion rate compared to the X-ray luminosity: assuming a distance of 7 kpc, we find a 1-100 keV luminosity of 6.3×10^{37} erg s^{-1} which corresponds to $\dot{M} = 3.3 \times 10^{17}$ g s^{-1} for unitary conversion efficiency

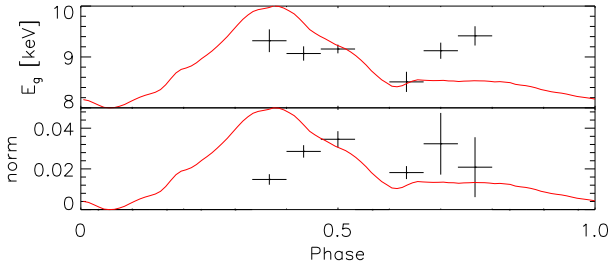

Figure 8. Best fit parameters for the Gaussian emission line as function of the phase. The line width is fixed to 1 keV. The solid line is the smoothed pulse profile in the 10–20 keV energy band with arbitrary normalization.

from gravitational to electromagnetic energy. If we consider only the BW component, we find $L_X = 5.5 \times 10^{37}\,\mathrm{erg\,s^{-1}}$ and $\dot{M} = 1.7 \times 10^{17}\,\mathrm{g\,s^{-1}}$. Our adopted value for $\dot{M}$ is instead $0.6 \times 10^{17}\,\mathrm{g\,s^{-1}}$, a factor three lower. However, using the relation $L_X = GM_*\dot{M}/R_*$, one assumes an isotropic emission over 4π steradians. This clearly overestimates the luminosity from a single magnetic pole by at least a factor of two. The factor could be even larger if the emission came from a fan beam geometry and/or the NS has a different mass to radius ratio. In general, the prescription for the calculation of the luminosity in X-ray pulsars probably needs to be re-examined and firmed up due to these expected anisotropies in the emission profile.

The most striking observational feature of 4U 0115+63 is the unique presence of at least five cyclotron lines in its spectrum; other HMXBs display at most a second, and in one case a third harmonic (see Coburn et al. 2002; Orlandini 2004; Tsygankov et al. 2006; Caballero et al. 2007). This is due to the relatively low intensity of its magnetic field, the lowest among the Galactic HMXBs that display cyclotron absorption features. In fact, at energies corresponding to the higher harmonics, there is still a high photon density, up-scattered in energy by the thermal population of electrons at a temperature of a few keV. The presence of the significant high-energy continuum allows the harmonic absorption features to be detected.

This peculiar characteristic finds some correspondence also in the continuum model. For example, we show for the first time that the high energy ($\gtrsim 10$ keV) emission of 4U 0115+63 is dominated by Comptonized cyclotron cooling, as expected on theoretical basis (Arons et al. 1987). Conversely, in Her X-1 and other X-ray pulsars with higher magnetic field, the emission is dominated by the Comptonized bremsstrahlung component (Becker & Wolff 2007). Using the best fit parameters obtained from the phase averaged spectrum, we simulated the source emission if the magnetic field were higher and found that the relative contribution of the cyclotron component decreases relative to bremsstrahlung and fades to a negligible value for $B \gtrsim 5 \times 10^{12}$ G. The reason is the decreased production rate for the cyclotron seed photons that form as a result of radiative de-excitation from the first excited Landau level, since this is less and less populated as its energy becomes higher than the electron temperature. As a consequence, the spectrum of this source is dominated by reprocessed cyclotron emission, in contrast to other bright pulsars with stronger magnetic fields, in which the emission is dominated by reprocessed bremsstrahlung emission (Becker & Wolff 2007).

Decomposing the contributions of the different components as functions of the phase demonstrates that along the peak, between 65% and 90% of the radiation is produced by the BW

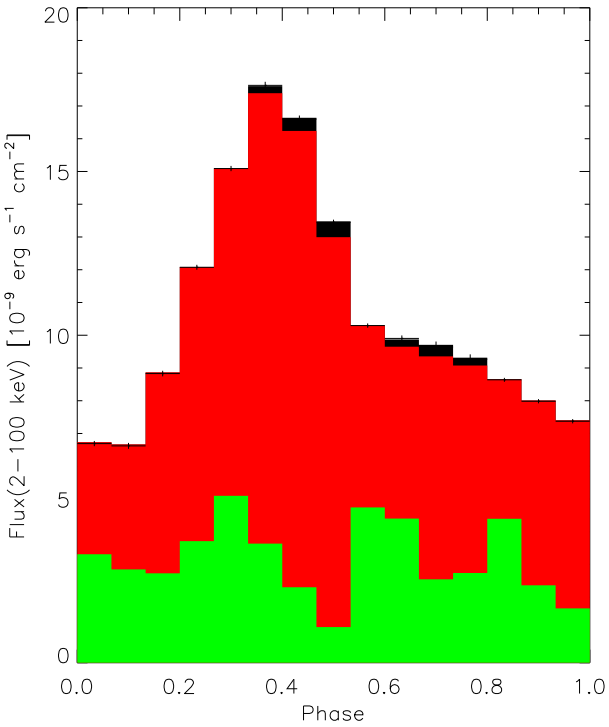

Figure 10. Contribution of the BW model plotted in red (dark gray), compTT in green (light gray), and the Gaussian emission line in black to the total flux (points with error bars).

component, while at other phases the relative contribution of the thermal Comptonization reaches ∼50% (Fig. 10). The contribution of the Gaussian emission line is always less than 5% and is concentrated on the descending part of the main peak. This is probably due to incomplete modeling of the cyclotron scattering process. The high energy component clearly originates in the accretion column while the low energy component has the characteristics of a diffuse halo, since its absolute flux is roughly constant throughout the phase.

5.1. Parameter constraints

During the determination of the optimal mass accretion rate, we noted that this parameter is tightly anti-correlated with the column radius, and both are linked to ξ via eq. (1). Since there is no basis for choosing a priori the value of ξ, it was necessary to study the probability contour plots of r_0 and $\dot{M}$ in the range $450\,\mathrm{m} < r_0 < 1100\,\mathrm{m}$ and $0.4 < \dot{M}_{17} < 1.1$, where $\dot{M}_{17}$ is the mass accretion rate in units of 10^{17} g/s. We found that at 68% c.l., any combination of these parameters is acceptable provided it falls between the lines of the equations $r_0 = 1250\,(\dot{M}_{17} - 0.56) + 450$ and $r_0 = 1823\,(M_{17} - 0.46) + 450$, where r_0 is expressed in meters. We then made the choice of fixing $\dot{M}_{17} = 0.6$ and $r_0 = 600$ m, the latter according to the indication of a relatively large column in other bright sources studied by Becker & Wolff (2007), and also based on the upper limit set by Lamb et al. (1973), and later revised by Harding et al. (1984).

We also verified that the NS mass and radius cannot be constrained by the spectral data. Any change in their value within reasonable boundaries can be compensated by tuning the mass accretion rate and column radius. Therefore, only four out of the

namely six free parameters can be determined by a direct fit of the model to the data. On the contrary, we already showed that we can constrain just a relatively wide region of the r_0–$\dot{M}$ plane, and this region depends on the particular choice of the NS base parameters. Among the free parameters, the magnetic field is insensitive to the choice of the fixed parameters, while ξ, δ and T_e depend on them. At least in the case of 4U 0115+63, where the lower energy portion of the spectrum is dominated by another component, it is not possible to infer from the data all the physical characteristics of the accretion column. Nevertheless, the BW model gives us the unique chance to investigate the basic emission mechanisms.

5.2. Magnetic field structure and emission geometry

The other main issue is the strength of the magnetic field producing the cyclotron emission, which is found to be $(0.60 \pm 0.06) \times 10^{12}$ G, while in the line forming region the field strength is 0.989×10^{12} G, as derived from the centroid energy of the second harmonic (the values are given neglecting the gravitational redshift, which acts as a scale factor). Assuming a dipolar field, and supposing that the cyclotron absorption features form close to the neutron star surface, we derive the cyclotron emission is concentrated at ∼1.7 km above the stellar surface. Based on this observation, we argue that the cyclotron cooling in 4U 0115+63 takes place between the NS and the column sonic point, which is at ∼2.7 km above the surface, according to the best fit model parameters. At that height, the emission is strongly beamed since the plasma speed is $v/c \sim 0.25$ and most of the radiation is emitted downwards, as predicted for an emitting charge in relativistic motion (see e.g. eq. 4.100 – 4.103 of Rybicki & Lightman 1979).

The radiation is subject to Compton reprocessing inside the accretion column, and it can subsequently escape from the sides only near the base, where the advection velocity decreases, and the density and temperature are higher. We can verify that for the best fit value of ξ, the diffusive escape time from the column is comparable to the free-fall time from the sonic point – see eq. (104) of Becker & Wolff (2007). Further confirmation of this scenario comes from the phase dependency of the parameters ξ and T_e, which are higher along the peak, implying respectively that the radiation traveled mostly parallel to the magnetic field, and that the visible layer is deeper in the column for this phase range. The sharp feature in the pulsed fraction (Fig. 2) at ∼ 20 keV also fits into the picture: while the emerging radiation is beamed roughly perpendicular to the column, the resonant scattering produces an isotropic emission which reduces locally the pulsed fraction.

The lower energy component is due to thermal Comptonization of seed photons with temperature $T_0 = (0.51 \pm 0.01)$ keV, which is not far from the temperature of the thermal mound probably present at the base of the column: according to the BW model of the high energy emission we find $T_{\rm Th} \sim 0.7$ keV. However, any attempt to fit the broad band spectrum using the BW model alone was unsuccessful due to the very low flux of the components originating from the blackbody and bremsstrahlung sources compared to the cyclotron one. As was already discussed, the effective radius of the blackbody photon source for the low energy `compTT` component is about 15 km (or 9 km considering the gravitational redshift). It is therefore likely that the low-energy radiation source resides close to the NS surface, perhaps in a diffuse halo. An optically thick atmosphere ($\tau \sim 20$) at a temperature of a few keV could be confined by multipolar or crustal components

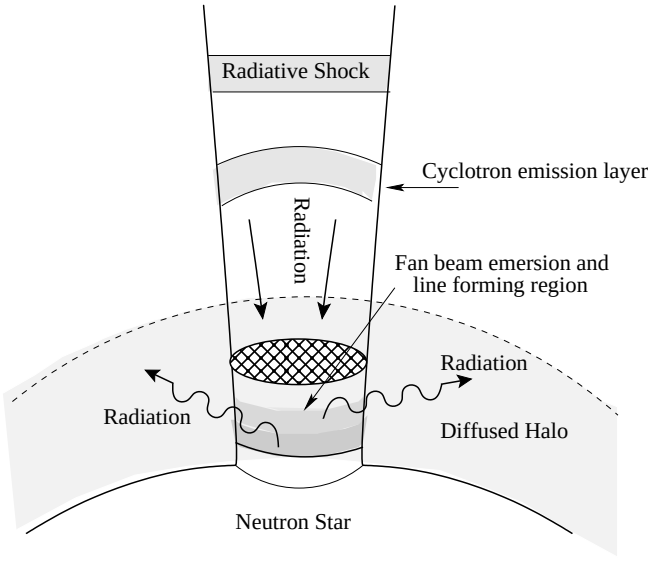

Figure 11. A schematic and not in scale cartoon of the magnetospheric structure of 4U 0115+63, as it emerges from our analysis.

of the magnetic field (see e.g. Gil et al. 2002), while the region around the column could be heated to ∼ 0.5 keV either by the accretion itself or by the strongly beamed column emission.

The modulation of the magnetic field producing the continuum radiation along the main peak (Fig. 6) suggests that the emission layer has not a planar geometry, but becomes closer to the NS at the edges of the column. A similar pattern is present in the phase dependency of the δ parameter, indicating that bulk Comptonization is stronger at the center of the main peak. The photon-diffusion parameter, ξ, follows nicely the pulse profile in the phase interval 0.2-0.8. This can give us some information on the angle between the magnetic field and the radiation direction.

Even though ξ is inversely proportional to the geometrical mean of the extreme values of the electron scattering cross section (see eq. [1]), and does not include explicitly its angle dependence, it can be regarded as an estimator of the average value in a particular phase bin. We argue that at the maximum of the peak, the radiation field is subject to a reduced scattering cross section, and therefore the photons must travel preferentially in the direction of the magnetic field lines (Ventura 1979). The photons are therefore able to reach almost the NS surface, before escaping from the column walls mostly near the base, where the plasma temperature is higher. At the column boundaries, where the plasma is optically thin outside the cyclotron resonances, the observed cyclotron absorption features are imprinted on the spectral energy distribution. In Fig. 11 we provide a schematic drawing of the model that we propose.

5.3. Standard spectral phenomenological model

Even though we were able to successfully model the continuum with a standard spectral phenomenological model similar to the one that Klochkov et al. (2008) used for EXO 2030+375, we consider this model unsatisfactory for 4U 0115+63 due to its incoherency with the pulse energy dependency. The pulse profiles and the pulsed fraction change at ∼ 7 keV, corresponding to the spectral region where the Gaussian “bump” starts to dominate, whilst they do not exhibit a peculiar evolution at the energy where the power law continuum becomes again the main

component. It is also difficult to explain why the same spectral component produces a pulsed fraction which is nearly constant below ∼ 5 keV and steadily increasing above ∼ 15 keV.

Adopting the spectral phenomenological model, we note the appearance of some residuals in the spectral fit below ∼ 1 keV (Fig. 3). Even though they are not statistically significant due to the low exposure of the *LECS* instrument, they essentially disappear when we adopt the multi-component Comptonization model (Fig. 4). With this latter model, we find that the photoelectric absorption due to neutral plasma is entirely due to the foreground Galactic medium: this is plausible since the observation took place after the outburst maximum when the strong radiation field of the NS could have ionized the surrounding medium.

Moreover, to our knowledge there is no physical process which could explain the broad Gaussian "bump" in emission: for instance, if it is due to cyclotron cooling, then one must find a way to make the Compton scattering so ineffective in reprocessing this component that it maintains a broad Gaussian profile instead of the typical power-law with exponential decay. We conclude that although this model can yield a good phenomenological description of the spectrum, it is nonetheless unable to give a coherent picture of the system in terms of physical processes.

The decoupling between the high and low energy emission is more naturally explained by two distinct emission components, one dominating below ∼ 7 keV, and the other above. In the scenario we have focused on here, the low energy emission (48% of the phase averaged total flux in the 1–100 keV energy band) is modeled as a thermal Comptonization of 0.51 keV seed photons (Titarchuk 1994), while the high energy continuum (51% of the total flux) is modeled using the BW formalism (Becker & Wolff 2007). We also add a Gaussian emission line which gives a minor contribution to the total flux (∼ 1%). The appearance of this component likely reflects either an approximation of the emission wings predicted to appear near the fundamental by Monte Carlo simulations of cyclotron scattering (Schönherr et al. 2007, and references therein), and/or an adjustment to the BW model to account for a more complex geometry in the scattering process. While this component is required to obtain an acceptable χ^2, it is clearly not a major contributor to the continuum, in contrast to the phenomenological model described above, in which it contributes 16% of the total flux in the 1–100 keV energy band.

5.4. Structure of the cyclotron harmonics

The line widths of the second and third harmonics reach a minimum just after the maximum of the pulse, which indicates that the line of sight reaches its maximum angle relative to the magnetic field at this phase. However, we note that the lines appear much shallower than those computed in the MC models (Schönherr et al. 2007). Probable reasons are a more complex geometry with respect to the model assumptions and general relativistic effects such as light bending, lensing effect, and doppler shift. A more quantitative discussion of this issue and the scenario we envisage for the system would require a complete numerical simulation, but this goes beyond the scope of the present paper.

If the radiation field dominates the thermodynamics of the plasma, then one expects a link between the temperature of the plasma and the magnetic field intensity. The relation depends on the optical depth in the absorption lines, the angle that the radiation forms with the magnetic field lines, and the system geometry (e.g. Isenberg et al. 1998, and references therein). In a slab geometry and for radiation injected parallel to the magnetic field, the cyclotron energy should be more than two times the plasma temperature. For isotropic radiation, one instead expects a ratio of about 4. This is the case for the halo temperature and the cyclotron line energy found here, while the column temperature is too high to be due to cyclotron heating, supporting the idea that the line forming region is not located within the column but rather in an external halo.

The apparent non-harmonicity of the line spacing in some HMXBs has been explained by the variation of the magnetic field in the line forming region. Nishimura (2003) showed that for a dipolar field the height of the region relevant for the absorption and scattering process must be of the order of several hundred meters to reproduce the observations. In a later work Nishimura (2005) demonstrates that a linearly varying magnetic field is able to produce line non-harmonicity even for a 5 m thick slab of plasma above the NS. Such a configuration can be modeled by a combination of axial and crustal magnetic field, as proposed by Gil et al. (2002).

We show that the higher harmonics are equally spaced in 4U 0115+63, as also noted by Santangelo et al. (1999) and Tsygankov et al. (2007), and therefore the field is nearly constant in the line forming region. The previously reported deviations from harmonicity regards only the ratio to the fundamental, whose centroid energy can be displaced from the cyclotron value. This can be due to the influence of the other emitting component, which is present below the cyclotron energy, and/or to a complex shape of the line profile, heavily modified by photon spawning, and then poorly described by a Gaussian absorption line. Also the need to introduce a Gaussian emission line points towards a complex structure of the cyclotron fundamental line, with emission wings that are not modeled by a Gaussian profile.

Using the second harmonic, with energy ∼ 20 keV, as the best estimator of the magnetic field in the line forming region, the displacement from the harmonic law is always less than 5% for the higher harmonics, thus the scattering region thickness is at most 2% of its distance from the NS center. The modulation of the line centroid energy with phase was already reported e.g. by Mihara et al. (2004) and is a typical feature of this source: it is interpreted as due to the occultation of part of the column by the NS along its rotation. Since the magnetic field of the line forming region varies from $(1.07 \pm 0.08) \times 10^{12}$ G to $(0.87 \pm 0.15) \times 10^{12}$ G along the main peak, the maximum reduction from the maximum value is 23%. This corresponds to an 8% variation of the height of the line forming region; assuming that at phase 0.5–0.6 the absorption takes place close to the base of the column and the NS has a radius of 10 km it means that for instance at phase 0.2–0.3 the scattering takes place in a layer, which is a few hundred meters thick, located ∼ 800 m above the NS surface.

The last issue we would like to briefly discuss is the puzzling jump of the energy of the fundamental cyclotron feature around the pulse minimum from ∼ 11 to ∼ 15 keV. A similar discontinuity was already noted in the phase averaged spectrum by Mihara et al. (2004); Nakajima et al. (2006); Tsygankov et al. (2007) when the luminosity drops below 5×10^{37} erg/s: it is interpreted as a drift of the compact emitting region in the magnetic field, due either to the disruption of the radiative shock or possibly to the accretion column burning out with the onset of another column in a multi-polar configuration. We show that this jump is not linked exclusively to the system luminosity, but appears at different phases even when the source is brighter than the proposed threshold for the shock disruption ($\sim 6 \times 10^{37}$ erg s^{-1}). Moreover, the absorption features at 30–40 keV which are present outside the main peak, do not seem to be linked by an harmonic ratio to the ∼ 20 keV line,

which suggests that complex field geometries could be present in 4U 0115+63.

6. Conclusions

For the first time we apply the self-consistent model of the high luminosity X-ray binary pulsar emission proposed by Becker & Wolff (2007) to the well studied transient source 4U 0115+63 during the giant outburst that occurred in 1999. We find that the emission of the peak is produced by thermal and bulk Comptonization of the cyclotron emission which is the main cooling channel of the column. On the other hand the lower energy continuum is roughly constant throughout the phase, and is due to thermal Comptonization of a 0.5 keV blackbody, whose effective radius is comparable to the NS dimensions.

We are able to sketch a model in which the photons are generated by cyclotron cooling well above the NS surface. The photons are advected towards the NS by the relativistic plasma bulk motion, while they are Compton up-scattered by the hot electrons in the column. The radiation escapes from the column lateral walls close to the NS surface, where the relativistic beaming is less severe. At this height the cyclotron lines are formed, probably in the boundary layer between the column and the plasma which forms an extended halo above the NS surface, and also produces the low-energy spectral component.

Unequivocal interpretation of the phase-dependent parameters using the theoretical model would require some estimate of the angles for the system. I.e., the angle between the line of sight and the rotation axis, and the angle between the rotation axis and the accretion column. These two angles would determine the portion of the column visible during a given phase, as well as the angle between the normal to the column and the line of site to the observer. Relativistic ray tracing should be used to study the influence of the system geometry on the emission pattern, but this is beyond the scope of this paper.

Although we have developed a convincing physical model for 4U 0115+63 which is able to describe coherently the system properties, we emphasize that this scenario should be checked quantitatively in future work using a detailed simulation. The analysis presented here was made possible via the implementation of the model proposed by Becker & Wolff (2007) in the standard fitting package `Xspec`. The application of this new model is very promising and it is expected to facilitate the study of many other systems.

Acknowledgements

The authors would like to thank M. Wolff for suggesting to us the possible anisotropy of the X-ray emission from the column, and also the referee M. Falanga who provided several insightful comments that led to significant improvements in the manuscript. C. F. has been supported by grant DLR 50 OG 0601 during this work.

References

Araya, R. A. & Harding, A. K. 1999, The Astrophysical Journal, 517, 334
Araya-Góchez, R. A. & Harding, A. K. 2000, *ApJ*, 544, 1067
Arnaud, K. A. 1996, Astronomical Data Analysis Software and Systems V, 101, 17
Arons, J., Klein, R. I., & Lea, S. M. 1987, Astrophysical Journal, 312, 666
Becker, P. A. & Wolff, M. T. 2007, The Astrophysical Journal, 654, 435
Boella, G., Butler, R. C., Perola, G. C., et al. 1997a, *A&AS*, 122, 299
Boella, G., Chiappetti, L., Conti, G., et al. 1997b, *A&AS*, 122, 327
Caballero, I., Kretschmar, P., Santangelo, A., et al. 2007, A&A, 465, L21
Coburn, W., Heindl, W. A., Rothschild, R. E., et al. 2002, The Astrophysical Journal, 580, 394
Cominsky, L., Clark, G. W., Li, F., Mayer, W., & Rappaport, S. 1978, *Nature*, 273, 367
Davidson, K. & Ostriker, J. P. 1973, *ApJ*, 179, 585
Dickey, J. M. & Lockman, F. J. 1990, *ARA&A*, 28, 215
Ferrigno, C., Segreto, A., Santangelo, A., et al. 2007, A&A, 462, 995
Frontera, F., Costa, E., dal Fiume, D., et al. 1997, *A&AS*, 122, 357
Giacconi, R., Gursky, H., Kellogg, E., Schreier, E., & Tananbaum, H. 1971, *ApJ*, 167, L67
Gil, J. A., Melikidze, G. I., & Mitra, D. 2002, *A&A*, 388, 246
Harding, A. K., Kirk, J. G., Galloway, D. J., & Meszaros, P. 1984, Astrophysical Journal, 278, 369
Heindl, W. A., Coburn, W., Gruber, D. E., et al. 1999, *ApJ*, 521, L49
in 't Zand, J. J. M., Verbunt, F., Strohmayer, T. E., et al. 1999, A&A, 345, 100
Isenberg, M., Lamb, D. Q., & Wang, J. C. L. 1998, The Astrophysical Journal, 505, 688
Johns, M., Koski, A., Canizares, C., et al. 1978, *IAU Circ.*, 3171, 1
Kalberla, P. M. W., Burton, W. B., Hartmann, D., et al. 2005, A&A, 440, 775
Klochkov, D., Santangelo, A., Staubert, R., & Ferrigno, C. 2008, A&A, 491, 833
Kraus, U., Zahn, C., Weth, C., & Ruder, H. 2003, The Astrophysical Journal
Kreykenbohm, I., Mowlavi, N., Produit, N., et al. 2005, *A&A*, 433, L45
Lamb, F. K., Pethick, C. J., & Pines, D. 1973, Astrophysical Journal, 184, 271, a&AA ID. AAA010.142.027
Manzo, G., Giarrusso, S., Santangelo, A., et al. 1997, *A&AS*, 122, 341
Mihara, T., Makishima, K., & Nagase, F. 2004, *ApJ*, 610, 390
Nakajima, M., Mihara, T., Makishima, K., & Niko, H. 2006, *ApJ*, 646, 1125
Negueruela, I. & Okazaki, A. T. 2001, A&A, 369, 108
Negueruela, I., Okazaki, A. T., Fabregat, J., et al. 2001, A&A, 369, 117
Nishimura, O. 2003, *PASJ*, 55, 849
Nishimura, O. 2005, *PASJ*, 57, 769
Orlandini, M. 2004, ArXiv Astrophysics e-prints, astro-ph/0402628
Parmar, A. N., Martin, D. D. E., Bavdaz, M., et al. 1997, *A&AS*, 122, 309
Pringle, J. E. & Rees, M. J. 1972, *A&A*, 21, 1
Rappaport, S., Clark, G. W., Cominsky, L., Li, F., & Joss, P. C. 1978, *ApJ*, 224, L1
Riffert, H., Klingler, M., & Ruder, H. 1999, Physical Review Letters
Rybicki, G. B. & Lightman, A. P. 1979, New York
Santangelo, A., Segreto, A., Giarrusso, S., et al. 1999, *ApJ*, 523, L85
Schönherr, G., Wilms, J., Kretschmar, P., et al. 2007, A&A, 472, 353
Sunyaev, R. A. & Titarchuk, L. G. 1980, *A&A*, 86, 121
Tamura, K., Tsunemi, H., Kitamoto, S., Hayashida, K., & Nagase, F. 1992, Astrophysical Journal, 389, 676
Tananbaum, H., Gursky, H., Kellogg, E. M., et al. 1972, *ApJ*, 174, L143
Titarchuk, L. 1994, *ApJ*, 434, 570
Tsygankov, S. S., Lutovinov, A. A., Churazov, E. M., & Sunyaev, R. A. 2006, Monthly Notices RAS, 371, 19
Tsygankov, S. S., Lutovinov, A. A., Churazov, E. M., & Sunyaev, R. A. 2007, Astronomy Letters, 33, 368, (c) 2007: Pleiades Publishing. Inc
Ventura, J. 1979, Physical Review D - Particles and Fields, 19, 1684, a&AA ID. AAA026.063.016
Wasserman, I. & Shapiro, S. L. 1983, Astrophysical Journal, 265, 1036
Wheaton, W. A., Doty, J. P., Primini, F. A., et al. 1979, *Nature*, 282, 240
White, N. E., Swank, J. H., & Holt, S. S. 1983, *ApJ*, 270, 711
Whitlock, L., Roussel-Dupre, D., & Priedhorsky, W. 1989, *ApJ*, 338, 381